

Imidazolium-Based Anion Exchange Membranes For Alkaline Anion Fuel Cells: Elucidation of the Morphology and the Interplay Between Morphology and Properties

Yue Zhao,^{1,*} Kimio Yoshimura,¹ Hideyuki Shishitani,² Susumu Yamaguchi,² Hirohisa Tanaka,² Satoshi Koizumi,^{3,*} Noemi Szekely,⁴ Aurel Radulescu,⁴ Dieter Richter,⁵ Yasunari Maekawa^{1,*}

¹*Quantum Beam Science Center (QuBS), Japan Atomic Energy Agency (JAEA), Tokai-mura, Ibaraki, 319-1195, and Watanuki-machi 1233, Takasaki, Gunma, 370-1292, Japan*

²*Daihatsu Motor Co., Ltd., Ryuo Gamo, Shiga 520-2593, Japan*

³*Department of Engineering, Ibaraki University, Hitachi 316-8511, Japan*

⁴*Forschungszentrum Jülich GmbH, Jülich Centre for Neutron Science @ MLZ, Lichtenbergstraße 1, D-85747 Garching, Germany*

⁵*Jülich Centre for Neutron Science & Institute for Complex Systems, Forschungszentrum Jülich GmbH, D-52425 Jülich, Germany*

*To whom all correspondence should be addressed: Yue Zhao (zhao.yue@jaea.go.jp); Yasunari Maekawa (maekawa.yasunari@jaea.go.jp); Satoshi Koizumi (skoizumi@mx.ibaraki.ac.jp)

ABSTRACT: We investigated the morphology and swelling behavior of a new graft-type of anion exchange membranes (AEMs) containing 2-methylimidazolium groups by using contrast variation small angle neutron scattering (SANS) technique. These AEMs were prepared by radiation-induced grafting of 2-methyl-1-vinylimidazole and styrene into poly(ethylene-co-tetrafluoroethylene) (ETFE) films and a subsequent *N*-alkylation with methyl iodide, and possessed both high alkaline durability and high conductivity. Our results showed that the crystalline lamellar and crystallite structures originating from the pristine ETFE films were more or less conserved in these AEMs, but the lamellar *d*-spacing in both dry and wet membranes were enlarged, indicating an expansion of the amorphous lamellae due to the graft chains introduced in the grafting process and the water incorporated in the swelling process. For the first time, the swelling behavior of the AEMs was studied quantitatively in various water mixtures of water and deuterated water with different volume ratios (contrast variation method), and the morphology of these membranes was elucidated by three phases: phase 1) crystalline ETFE domains, which offer good mechanical properties; phase 2) hydrophobic amorphous domains, which are made up of amorphous ETFE chains and offer a matrix to create conducting regions; phase 3) interconnected hydrated domains, which are composed of the entire graft chains and water and play a key role to promote the conductivity.

I. Introduction

In the previous study, we reported the synthesis and characterization of a series of newly developed imidazolium cation based anion exchange membranes (AEMs) made by radiation-induced grafting of 1-vinylimidazole and styrene into poly(ethylene-co-tetrafluoroethylene) (ETFE) films, and followed by *N*-alkylation with methyl iodide.¹ These AEMs were characterized to be terpolymers, and showed better alkaline durability in 1 M KOH at 80 °C. Most lately, we further modified the grafted imidazole group to 2-methyl-1-vinylimidazole, and the resultant AEMs (hereafter named 2Me-AEM) exhibit even higher ion conductivity (> 100 mS/cm) and longer alkaline durability, owing to the fact that the methyl protecting group at 2-imidazole position prevent the ring-opening degradation. 2Me-AEM with an *IEC* (ion exchange capacity) of 1.82 mmol/g shows the best well-balanced properties required for fuel cell applications. All these findings on one hand, are a result of sample preparation procedure of the radiation grafting method and the introduction of alkyimidazolium cations as an anion conducting group, and on the other hand, is believed to be controlled by the microphase separated structures of the membranes in the hydrated state, though the precise manifestation of which was unclear. In this work, we aim to advance the work, elucidate the morphology of these 2Me-AEMs and understand the structure related unique properties such as the mechanical property and the anion conductivity.

Due to the growing concerns on the depletion of petroleum based energy resources and the climate change, polymer electrolyte membrane fuel cells (FCs) technologies have received much attention in recent years owing to their high efficiencies and low emissions.²⁻¹² Among them, hydrogen-type FCs which use proton exchange membranes (PEMs) have been heavily studied due to their feature of low operating temperature, high current density and fast start-ups.¹⁰⁻¹² However, PEM-FCs need to work in highly acidic environment to promote high proton conductivity, which requires the consumption of acid-resistant precious metal catalysts and costs up. In order to solve this problem, alkaline anion exchange membrane fuel cell

(AEM-FC) is a good solution, in which oxygen reduction reaction kinetics at the cathode are much more facile than in PEM-FCs under alkaline conditions, potentially allowing the use of inexpensive, non-noble metal catalysts such as nickel, cobalt or iron particles for the cathode and nickel for the anode.¹³⁻¹⁵

Although AEM-FCs exhibit above potential advantages, the biggest challenge in developing AEM-FCs is to fabricate AEM with high ion conductivity and mechanical stability without chemical deterioration at elevated pH and temperatures. So far, most strategies were focused on synthesizing new thermally and chemically durable fluorinated and aromatic polymers¹⁶⁻¹⁸. For the first time, our group tried to develop the new type of 2Me-AEMs by radiation grafting of imidazole/styrene on the mechanically tough poly(ethylene-co-tetrafluoroethylene) (ETFE) films.^{1,19} There have been intensive reports including our previous studies²⁰⁻²² on the radiation grafting technique, which has been successfully applied for the preparation of PEMs, where grafts containing an ion-conducting group (i.e. sulfonic acid) grafted onto fluorinated polymer films such as cross-linked polytetrafluoroethylene (cPTFE), ETFE, and poly(vinylidene fluoride) (PVDF) or fully aromatic hydrocarbon polymers such as poly(ether ether ketone).²⁰⁻²⁹ Therefore, we believe that this technique may allow the introduction of large amount of grafts containing ion-conducting groups into the AEMs, thus the resultant AEMs are expected to possess both high ion conductivity and good mechanical properties.

It is generally accepted that the properties of membranes derive from the microphase separation of hydrophilic ionic material from the hydrophobic substance. Therefore, to design new AEMs, one should not only consider the architecture of the molecule itself, but also understand the microphase separation structures of membranes, such as the crystalline domains, the formation of conducting regions, and the distribution of ionic groups and water in the conducting regions. The morphology of crystalline domains for polystyrene-grafted PEMs prepared by the radiation grafting technique has been intensively investigated using

differential scanning calorimetry (DSC), X-ray diffraction (XRD) and small-angle scattering methods.²⁰⁻²⁹ For instance, the crystallinity of the grafted films was found to decrease with an increase in grafting degree by many researchers in different fluoropolymers bases.²⁷⁻²⁹ In our previous work, we studied the hierarchical structure of PEMs consisting of poly(styrenesulfonic acid) and PTFE base by using small angle neutron scattering (SANS) and small-angle X-ray scattering (SAXS) methods. The structure of these PEMs was characterized as being composed of conducting layers (graft domains) in lamellar stacks with 48-57 nm spacing on the surface of 480 nm diameter crystallites and ultrasmall structures with 1.7 nm correlation distance of sulfonic acid groups in the conducting layers.^{20,21} Most recently, we investigated the hierarchical structures of graft-type ETFE-based PEMs by using Ultra-SAXS technique, and found that when *IEC* is low, the conducting graft domains are around the ETFE lamellar crystals, however, when *IEC* is high, new amorphous hydrated and crystallite network domains are formed independently.²²

According to the previous studies on graft-type PEMs, ETFE was regarded as the most promising base materials because of its well-balanced properties. Thus, we selected ETFE as the base material to develop the new type of imidazolium cation-grafted AEMs.¹ These AEMs, on one hand, are expected to form interconnected hydrophilic microdomains with ion transport channels, swelling in water to promote the ion conductivity; and on the other hand, their hydrophobic crystalline domains originating from pristine ETFE membranes are expected to provide the mechanical strength and restrict the dimensional changes upon swelling.

In this paper, we focus on the elucidation of the morphology of 2Me-AEMs by using contrast variation SANS method. Note that this is the first study on the graft-type AEMs material prepared by radiation grafting technique, and for the first time, we employ the contrast variation SANS method to quantitatively analyze the structure of these AEMs.

II. Experimental

II-1, Sample preparation and characterizations. 2Me-AEMs were prepared by radiation-induced grafting of 2-methyl-1-vinylimidazole and styrene into poly(ethylene-co-tetrafluoroethylene) (ETFE) films followed by *N*-alkylation with methyl iodide. The molecular structure is schematically shown in scheme 1. The sample preparation process is briefly described below: Firstly, pristine ETFE membranes with a thickness of 50 μm (Asahi Glass Co. Ltd., mass density (d_{ETFE}) = 1.75 g/cm^3 , crystallinity (X_c) = 0.32) were irradiated by a ^{60}Co γ -ray source (JAEA Takasaki, Gunma, Japan) with a total dose of 50 kGy under argon atmosphere; Secondly, these pre-irradiated membranes were immersed in argon-purged monomer mixture solution of 2-methyl-1-vinylimidazole and styrene (9/1 v/v) to obtain grafted-ETFE membranes; Finally, grafted-ETFE membranes were immersed in the 1M 1,4-dioxane solution of methyl iodide and then soaked in a hydrochloric acid solution followed by a sodium bicarbonate solution to get *N*-alkylated 2Me- AEMs. Note that the counter-ions in AEMs have been converted from iodide to bicarbonate forms in the final step to prevent degradation, which is often observed with the hydroxide form. The details of the radiation grafting method and preparation conditions can be found elsewhere.^{1,19} The ion exchange capacity of the 2Me-AEMs was determined by standard back-titration analysis.¹ Because of the best performance in the direct hydrazine hydrate fuel cell test, the structure of 2Me-AEMs with an *IEC* of 1.82 mmol/g is targeted to be comprehensively studied in the following sections.

The grafting degree (*GD*) of these 2Me-AEMs (*IEC*~1.82 mmol/g) is 91%, estimated by the following eq. (1)

$$GD(\%) = \frac{W_g - W_0}{W_0} \times 100\% \quad (1)$$

where W_0 and W_g are the weights of the membranes before and after grafting in the dried state, respectively. The molar ratio of 2-methyl-1-vinylimidazole to styrene units in the grafts was

estimated by gravimetric changes between grafted-ETFE membranes and chloride forms of 2Me-AEMs, given that the *N*-methylation of imidazole units in the graft-copolymer proceeded quantitatively. The molar ratio of imidazole to styrene units in AEM calculated to be 64:36. Thus, the mass density of the grafts (d_{graft}) can be calculated to be $\sim 0.98 \text{ g/cm}^3$ on the basis of the reported mass densities of polystyrene and poly(*N*-vinylimidazole) homo-polymers being 1.05 and 0.95 g/cm^3 , respectively.

Fully water-swollen membranes were simply prepared by immersing the dry 2Me-AEMs into water at 25 °C. The water-uptake U , is determined by the weight measurements using eq. (2) below.

$$U = \frac{W_{\text{wet}} - W_{\text{dry}}}{W_{\text{dry}}} \times 100\% \quad (2)$$

where W_{wet} and W_{dry} represent the weight of 2Me-AEMs in the fully wet and dry states, respectively. In this study, U of 2Me-AEMs ($IEC \sim 1.82 \text{ mmol/g}$) is estimated from H_2O -swollen membranes to be 48%, where the mass density of water (d_w) is 1.0 g/cm^3 . Thus, the total water volume fraction (ϕ_w) of wet AEMs can be calculated by eq. (3) below

$$\phi_w = \frac{\frac{U/100(1+GD/100)}{d_w}}{\frac{1}{d_{\text{ETFE}}} + \frac{GD/100}{d_{\text{graft}}} + \frac{U/100(1+GD/100)}{d_w}} \quad (3)$$

to be ~ 0.38 . Similarly, the volume fraction of ETFE ($\phi_{\text{ETFE}} = \frac{\frac{1}{d_{\text{ETFE}}}}{\frac{1}{d_{\text{ETFE}}} + \frac{GD/100}{d_{\text{graft}}} + \frac{U/100(1+GD/100)}{d_w}}$)

and grafts ($\phi_{\text{graft}} = \frac{\frac{GD/100}{d_{\text{graft}}}}{\frac{1}{d_{\text{ETFE}}} + \frac{GD/100}{d_{\text{graft}}} + \frac{U/100(1+GD/100)}{d_w}}$) in the wet state can be deduced as well.

Thus, the volume fraction of crystalline ETFE ($\phi_{\text{cry_ETFE}}$) and amorphous ETFE ($\phi_{\text{amo_ETFE}}$) can be estimated by considering X_c : $\phi_{\text{cry_ETFE}} = X_c \times \phi_{\text{ETFE}}$ and $\phi_{\text{amo_ETFE}} = (1 - X_c) \times \phi_{\text{ETFE}}$, respectively. Furthermore, according to the ratio of 2-methyl-1-vinylimidazole to styrene units (64:36) on the grafts, the volume fraction of imidazole (ϕ_{im}) and styrene (ϕ_{st}) segments can also be roughly estimated to be $\phi_{\text{im}} = 0.64 \times \phi_{\text{graft}}$ and $\phi_{\text{st}} = 0.36 \times$

ϕ_{graft} , respectively. The volume fraction of each component in the fully water-swollen AEMs is summarized in Table 1.

Note that we also prepared 2Me-AEMs having an Im/St ratio of c.a. 65:35 with GDs of 30, 46 and 120% by the same procedure as 2Me-AEM with a GD of 91% mentioned above to investigate the effect of GDs on the electrochemical properties and hierarchical structures. The preparation and characterization of these membranes will be reported in detail elsewhere for discussion of the fuel cell performance and durability of 2Me-AEMs.

II-2. Small-angle Neutron Scattering (SANS) measurement. SANS measurements were performed mainly on KWS-2 SANS diffractometer operated by Juelich Centre for Neutron Science at the neutron source Heinz Maier-Leibnitz (FRM II reactor) in Garching, Germany.³⁰ The incident neutron beam at KWS-2 was monochromatized with a velocity selector to have the average wavelength (λ) of 5 Å with a wavelength resolution of $\Delta\lambda / \lambda = 20\%$. The scattering patterns were collected with a two-dimensional scintillation detector, and circularly averaged to obtain scattering intensity profiles as a function of q , where q is the scattering vector, defined by $q = (4\pi/\lambda)\sin(\theta/2)$, with λ and θ being the wavelength of the neutron and the scattering angles, respectively. Part of SANS measurements were also done on IBARAKI Materials Design Diffractometer (iMATERIA) at the Japan Proton Accelerator Research Complex (J-PARC), Japan,³¹ where the SANS instrument has four detector banks and covers a wide q range from 0.02 to 40 Å⁻¹ with gradually changing resolution. The obtained scattering profiles were corrected for the instrument background, detector sensitivity, and scattering from empty cell, and finally calibrated to absolute scale (cm⁻¹) using a Plexiglas secondary standard. The scattering intensity profile of each water mixture of H₂O and D₂O was measured in a quartz cell with a thickness of ~ 0.5 mm, and used to estimate the incoherent scattering intensity for each water-swollen membrane with respect to its thickness. The estimated incoherent scattering intensity was subtracted from the absolute scattering intensity of each profile. All of the measurements were done at 25 ± 0.5 °C.

II-3. Electrochemical Impedance Spectroscopy. In-plane anionic conductivity was calculated using electrochemical impedance spectroscopy (EIS) to measure membrane resistance. The membrane was mounted in a four-electrode test cell, with platinum electrodes that are separated by a constant distance l . Impedance spectra were obtained over a frequency range greater than 1.0 kHz. EIS data were collected using a LCR meter (HIOKI 3522).¹ All the AEMs were fully hydrated in nitrogen-saturated deionized water, and the conductivity measurements were carried out in a beaker filled with nitrogen-saturated deionized water at 60°C. The ionic conductivity σ (mS cm⁻¹) of a given membrane can be calculated by $\sigma = l/(S \times R) \times 10^3$, where l is the distance between two electrodes (cm), S is the cross-section area of the membrane (cm²), and R is the membrane resistance (Ω).

III. Results

III-1, Grafting, alkylation and swelling effects on the morphology of the membranes.

After grafting and alkylation, the ion conducting groups in AEMs are formed. When such a dry AEM is immersed in water, the hydrophilic chains with imidazolium cation groups can absorb water and form interconnected ion channels in hydrated regions, where the ions are able to be transported, hence the ion conductivity is created. In order to improve the ion transport efficiency, the understanding of the grafting, alkylation and swelling effects on the morphology of the membranes is very crucial. In this section, we compare the SANS profiles of the dry pristine ETFE membranes (profile 1, squares), dry grafted-ETFE membranes (profile 2, circles), dry 2Me-AEMs (profile 3, down-triangles) and AEMs equilibrated in D₂O (profile 4, up-triangles) in Figure 1, and report how the morphology of the membranes changes during these processes.

III-1.1 Grafting effects. It is well known that the grafted ETFE membranes more or less maintain the crystalline structures of precursor ETFE membranes,^{22,32,33} hence the comparison between profile 1 before the grafting procedure and profile 2 after the grafting procedure indicates the morphology changes are related to the local lamellar stacking and distribution of

the crystallite grains induced by grafting effects.

Both the intensity and the shape of the profiles varied significantly upon grafting. Before grafting, the scattering intensity, $I(q)$, of profile 1 is relatively weaker than that of profile 2 and the other profiles, however, a clear upturn in the small q range at $q < 0.2 \text{ nm}^{-1}$ and a profound scattering maximum at $q = 0.31 \text{ nm}^{-1}$ are observed, indicating the typical crystalline ETFE lamellar structure with a d -spacing ($=2\pi/q$) of 20.0 nm as shown in Figure 2(a). This result is very much consistent with the previously reported data measured by SAXS method.^{22,32,33}

After grafting, profile 2 shows two broad scattering maxima: One maximum appears at $q_1 = 0.21 \text{ nm}^{-1}$ ($d_1 = 2\pi/q_1 \sim 30 \text{ nm}$), corresponding to the low- q shift of the crystalline peak observed in profile 1. This larger d -spacing indicates the expansion of the lamellar stacks compared to that in the pristine ETFE membranes due to the incorporation of the graft chains in the lamellar amorphous domains; The other maximum which appears at $q_2 = 0.035 \text{ nm}^{-1}$ ($d_2 = 2\pi/q_2 \sim 180 \text{ nm}$), represents the average distance between two grains, which are composed of crystalline ETFE regions and graft chains incorporated amorphous ETFE regions as shown in Figure 2(b). Note that Tap et al.²² even found an ambiguous peak in the ultra-small angle range at $q_s \sim 0.006 \text{ nm}^{-1}$ ($d_s \sim 1050 \text{ nm}$) for the polystyrene grafted ETFE films, and they attributed d_2 and d_s to the short and long periods of the crystallites. Since the same pristine ETFE material and similar grafting procedures were used in this study, a related peak around q_s might also exist though this q -range was not covered in the current SANS experiment.

It should also be noted that though the crystalline peaks in profile 2 (profiles 3 and 4 as well) are broad, they can certainly be identified. Generally, semicrystalline polymers³⁴⁻³⁶ like poly(ether ether ketone) (PEEK), with low grafting or sulfonation degree,³⁷ usually exhibit clear scattering maxima attributed to crystalline domains. The crystallinity index decreases with the sulfonation degree significantly. For instance, sulfonated PEEK membranes are reported to be amorphous when a sulfonation degree is over 50%.³⁸ Similarly, the broadening

of crystalline peaks in profiles 2-4 supports the idea that the grafted ETFE membranes and AEMs have lower crystallinity than pristine ETFE membranes. This conclusion is confirmed by DSC measurement. Surprisingly, the crystalline structure is conserved in the grafted ETFE and AEMs even when the grafting degree is as high as 91%. Previous studies on the ETFE-based PEMs prepared by radiation technique also showed the conservation of the crystalline structure when the grafting degree is above 100%.²² All these results proved that the irradiation grafting method is an efficient way to maintain the inherent characteristics of the substrates such as the crystallinity index and hence the mechanical strength, which offers new opportunities for the material development.

According to the scattering theory,³⁹ $I(q)$ of the membranes is proportional to the square of the scattering contrast, which is the difference in the scattering length density (SLD) between crystalline and amorphous domains. Hence the weaker $I(q)$ of profile 1 in comparison to that of profile 2, reveals a smaller scattering contrast between the ETFE crystalline regions and amorphous regions than that between the ETFE crystalline regions and grafts incorporated amorphous regions. In order to verify this point, we should estimate SLD of each component in the membrane theoretically as below.

SLD of a molecule of i atoms is related to its molecular structure and may be readily calculated from the simple expression given by $b = \sum_i b_i \frac{dN_A}{M_w}$ where b_i is the scattering length of i th atom, d is the mass density of the scattering body, M_w is the molecular weight, and N_A is the Avogadro constant.³⁹ Thus, SLD of imidazole (b_{im}) and styrene (b_{st}) segments on graft chains, and amorphous ETFE chains (b_{amo_ETFE}) are calculated to be 1.123, 1.415 and $2.0 (\times 10^{10} \text{ cm}^{-2})$, respectively.⁴⁰ SLD of crystalline ETFE (b_{cry_ETFE}) cannot be theoretically estimated so far, because their mass density is unknown, which heavily depends on the crystallinity and crystallization process in the membrane processing. However, a relatively higher value of b_{cry_ETFE} than b_{amo_ETFE} is expected due to the larger mass density of crystalline

ETFE than that of amorphous ETFE even having the same chemical structure. Obviously, the incorporation of graft chains may decrease the average SLD of amorphous regions (b_{amo}) and hence increase the scattering contrast between crystalline ETFE and amorphous regions, which explains the enhanced scattering intensity of the grafted membranes. The SLD value of each component was also listed in Table 1. Note that $b_{\text{cry_ETFE}}$ can be experimentally deduced by contrast variation SANS method, which will be further discussed in Section IV-1 in conjunction with Figure 6.

The upturn at $q < 0.2 \text{ nm}^{-1}$ in profile 1, reflects the large length scale morphology of the pristine ETFE sample. We notice that $I(q)$ and q follow power-law functions at different q -ranges: At $q < 0.14 \text{ nm}^{-1}$, a typical Porod law for smooth surfaces is observed, *i.e.* $I(q) \sim q^{-4}$,⁴¹ which is due to the scattering from the smooth surface of the crystallites or grains; At $0.14 \text{ nm}^{-1} < q < 0.2 \text{ nm}^{-1}$, a power law shows $I(q) \sim q^{-1}$, indicating crystalline lamellar domains are rod-like, within which a typical lamellar periodical spacing was found to be 20 nm as we mentioned above. Note that though the q -region where the power law exponent of -1 was observed is narrow, it seems a common characteristic for fluoropolymer membranes. The same change in the power law exponent from -1 to -4 with an increase in q was reported by Song et. al. for the pure ETFE film using SAXS method.²⁹ The very similar patterns in SANS profiles were also found in other fluoropolymer films such as PTFE and poly(tetrafluoroethylene-co-hexafluoropropylene) (FEP).^{21,27}

It should be noted that Porod law is observed at high- q regions of the profiles for both pristine membranes and grafted membranes, arising from the sharp interface between amorphous and crystalline lamellae. This Porod region is also found to shift toward low- q range in the grafted membranes, evidencing the expansion of the amorphous lamellae due to the grafting effect.

III-1.2 Alkylation effects. After alkylation, the SANS profile 3 exhibits very similar scattering pattern to that of the grafted ETFE membranes (profile 2) throughout the q -range,

demonstrating that the alkylation procedure induces little change in the correlation distance of the lamellar stacks and crystallites. Thus, it may be concluded that the distribution of grafted chains composing of both imidazole and styrene segments, which act as ion conducting channels, are decided during the radiation-induced grafting step, not the alkylation step. In other words, the morphology and property of the AEMs are determined by the grafting step, such as irradiation time, monomer species and amount, and reaction time, instead of alkylation step. Similar results have been also reported by Tap et al. in the polystyrene grafted PEMs, where they claimed that the sulfonation procedure affects little the structure of PEMs.²²

III-1.3 Swelling behavior of AEMs Equilibrated in water. SANS profile for the fully D₂O-swollen 2Me-AEMs is also shown in Figure 1 (profile 4). We observe that: 1) $I(q)$ of profile 4 is much larger than all the other three profiles throughout the whole q range. Note that water has been absorbed until saturation around hydrophilic grafts with a total U value of 48% to form hydrated regions. The scattering contrast between the crystalline ETFE regions and water incorporated amorphous regions is more enhanced because the absorbed heavy water has a much higher SLD, which increases the averaged SLD of the hydrated regions effectively.⁴⁰ Therefore, $I(q)$ of profile 4 is more enhanced.

In addition to the change in $I(q)$ described above in 1), we also observe the following changes in the shape of profile 4 arising from the swelling effects: 2) the two broad peaks shift more toward the low- q range at $q_1 = 0.185 \text{ nm}^{-1}$ and $q_2 = 0.0315 \text{ nm}^{-1}$, revealing the further expanded lamellar d -spacing (d_1) of 34 nm, and the inter-grain distance (d_2) of 200 nm in the presence of water. Unlike in the alkylation process, the expansion of both d_1 and d_2 upon swelling is obvious, indicating that the incorporation of water in the hydrophilic graft domains does enlarge the total lamellar spacing as shown in Figure 2(c). 3) Contrary to all the other three profiles, profile 4 shows a clear deviation from Porod law at $q > 1.4 \text{ nm}^{-1}$, in the length scale within the amorphous lamellae. It indicates the excess scattering arising from the

hydrated ion channels composed of hydrophilic graft chains and water. This excess scattering intensity varies when the water solvent is changed from pure D₂O to partially deuterated water, due to the changeable scattering contrast between the water and hydrophilic graft chains. We will discuss these results further in conjunction with contrast variation SANS results in section III-2 and IV.

III-2, Polymer-solvent contrast variation. In this section, contrast variation SANS measurements on the AEMs, which are equilibrated in water mixtures of water (H₂O) and deuterated water (D₂O) with different volume fraction of D₂O, f_{D2O} , were performed.

Note that the SLD of the water mixture (b_w) is a function of f_{D2O} given by

$$b_w = b_{D2O}f_{D2O} + b_{H2O}(1 - f_{D2O}) \quad (4)$$

where b_{D2O} and b_{H2O} are SLD of D₂O and H₂O, respectively.⁴⁰ Thus b_w is tunable in the contrast variation experiments, therefore, the hydrated regions may match to: 1) the crystalline ETFE domains at $f_{D2O} = m_1$, hence the scattering profile at m_1 represents the only visible hydrophobic amorphous domains; or 2) the hydrophobic amorphous domains at $f_{D2O} = m_2$, hence the scattering profile at m_2 represents the only visible crystalline ETFE domains. m_1 and m_2 are defined as the matching points where the scattering contrast between hydrated regions and crystalline ETFE domains or hydrophobic amorphous domains is minimum.

The representative scattering profiles of AEMs swollen in different water mixtures are shown in Figure 3. Apparently, both the intensity and shape of the profiles change as a function of f_{D2O} . Since the structure of the AEM itself is believed to be invariant whether the solvent is water or deuterated water, the apparent change in the profiles at different scattering contrast reflects either all or partial structure information of the membranes. According to the shape of the profiles and the dependency of the scattering intensity on f_{D2O} , the scattering profiles are classified into two q -regions: q -region I ($q < 0.3 \text{ nm}^{-1}$) and q -region II ($q > 0.3 \text{ nm}^{-1}$).

In q -region I, $I(q)$ decreases with the increasing f_{D2O} up to 55% and then increases again

from 55 to 100%. The two typical crystalline peaks representing the crystalline structure of the membranes are clearly observed in all profiles, except for that at $f_{D2O} = 55\%$. At $f_{D2O} = 55\%$, the crystalline peaks are invisible, indicating the crystalline domains have been matched by the hydrated regions, namely, approaching the matching point of m_1 . To quantitatively determine the matching point of m_1 , the scattering maxima at $q_I (= 0.185 \text{ nm}^{-1})$, $I(q_I)$, was plotted as a function of f_{D2O} for all contrasts in Figure 4a. m_1 at which a minimum $I(q_I)$ shows up has been thus determined to be 55%. The schematic illustration for the phase matching at m_1 has been shown in the inset of Figure 4a. The hydrated regions and crystalline ETFE regions are painted in the same color, demonstrating that the two phases have the same SLD, and there is no scattering contrast between them. Thus the AEM at m_1 is apparently a two-phase system composed of the hydrated phase (together with crystalline ETFE phase) and the hydrophobic amorphous phase.

In region II, $I(q)$ decreased with increasing f_{D2O} up to 40% and then increased again when f_{D2O} increases from 40 to 100%. The excess scattering at high- q range are clearly observed in all profiles, except for that at $f_{D2O} = 40\%$, indicating the formation of hydrated regions in the water-swollen AEMs. However, it is invisible at $f_{D2O} = 40\%$, instead, a Porod law behavior is clearly observed, indicating the amorphous hydrophobic domains have been matched by the hydrated regions, namely, approaching the matching point of m_2 . To determine m_2 , the apparent excess scattering intensity at a characteristic $q_{II} (= 2.0 \text{ nm}^{-1})$, $I(q_{II})$, was plotted as a function of f_{D2O} for all contrasts in Figure 4b. m_2 at which a minimum $I(q_{II})$ shows up has been thus determined to be close to 40%. The schematic illustration for the phase matching at m_2 was shown in the inset of Figure 4b. The hydrated regions and hydrophobic amorphous regions are painted in the same color, demonstrating that the scattering contrast between these two phases is very small, namely, the whole amorphous regions are forming one phase. Thus the AEM at m_2 is apparently a two-phase system composed of the crystalline ETFE phase and the entire amorphous phase.

IV. Discussion

IV-1 Determination of the components of the hydrated regions. From the contrast variation results in Figure 3, we noticed that all the profiles in Region I, except for the profile at the matching point of m_1 ($f_{D2O}=55\%$), seemed to be very similar to each other. When we normalized the scattering profiles to be superposed around the typical crystalline peak at q_I ($= 0.185 \text{ nm}^{-1}$), $I(q)$ depends only on the contrast factor as clearly seen in Figure 5. Accordingly, the system can be analyzed as a two-phase system, composed of crystalline ETFE domains and amorphous domains. The entire amorphous domains are regarded as one phase, consisting of hydrated regions and hydrophobic regions, both of which contribute to the total scattering intensity. Note that the deviations in high- q Region II due to scattering from the microphase separated structures within the amorphous lamellae was ignored in this section, but will be discussed in detail in later section IV-4.

For a two-phase system, the scattering intensity at q_I , $I(q_I)$, which experimentally readable, is proportional to the square of scattering contrast (Δb^2) between the ETFE crystallites phase (b_{cry_ETFE}) and the entire amorphous phase (b_{amo}), given by

$$I(q_I) \sim (b_{cry_ETFE} - b_{amo})^2 \quad (5)$$

The right hand side of eq. (5) can be theoretically calculated in terms of b_{cry_ETFE} and b_{amo} , which are independently determined at each f_{D2O} . Note that b_{amo} can be uniquely calculated as a function of f_{D2O} regardless of the components of the hydrated region (e.g., graft chains including imidazole and styrene segments and water) as shown in the equation below

$$b_{amo} = \frac{\phi_{amo_ETFE} b_{amo_ETFE} + \phi_{st} b_{st} + \phi_{im} b_{im} + \phi_w b_w}{\phi_{amo_ETFE} + \phi_{graft} + \phi_w} \quad (6)$$

all the parameters in eq. (6) can be found in Table 1, except for b_w , which is a function of f_{D2O} , and can be calculated by eq. (4).

On the contrary to b_{amo} , it is difficult to determine b_{cry_ETFE} theoretically, however, we have experimentally found that at the matching point of m_1 ($f_{D2O} = 55\%$), $b_{cry_ETFE} \approx b_{hydra}$,

where b_{hydra} is the averaged SDL of the hydrated regions. The estimation of b_{hydra} at m_1 offers a way to quantitatively determine $b_{\text{cry_ETFE}}$. To estimate b_{hydra} , we have to know the components of hydrated regions. Only if we find the correct composition in the hydrated region, the plot of $I(q_1)$ as a function of $(b_{\text{cry_ETFE}} - b_{\text{amo}})^2$ in eq. (5) will give a linear relationship. Based on this strategy, we successfully determined that the hydrated regions are composed of the entire graft chains and water as shown in the inset of Figure 6, and $b_{\text{cry_ETFE}}$ is $2.23 \times 10^{10} \text{ cm}^{-2}$ (listed in Table 1). A good linear relationship between $I(q_1)$ and $(b_{\text{cry_ETFE}} - b_{\text{amo}})^2$ is shown in Figure 6, verifying not only the correctness of $b_{\text{cry_ETFE}}$ but also the components of the hydrated regions. The model analysis with various components of the hydrated regions can be found in the supporting information, in conjunction with Figures S1, S2 and S3.

IV-2 Morphology of Amorphous ETFE domains. Since the hydrated regions are made of the entire graft chains and water, the matching at m_1 ($f_{\text{D2O}} = 55\%$) makes hydrophobic amorphous ETFE domains the only visible component. Thus, the scattering profile at m_1 , $I_{m1}(q)$, represents the morphology of hydrophobic amorphous ETFE chains. We extract $I_{m1}(q)$ and plot it in Figure 7a.

At $q > 0.09 \text{ nm}^{-1}$, the scattering profile can be well fitted by Debye function for random polymer coils as show in eq. (7) below

$$I(q) = \frac{2}{x^2} [\exp(-x) - 1 + x] \quad (7)$$

where $x = (qR_g)^2$, with R_g being the radius of gyration of the polymer chains. The best-fitted theoretical curve (solid line) is presented in the figure as well, and the resultant R_g is 7.6 nm. It indicates that in the amorphous regions, the ETFE polymers adopt the more or less random-coil structure with an average $R_g \sim 7.6 \text{ nm}$. The absorbed dose employed here (50 kGy) is not high enough to cause scission or crosslinking to ETFE polymer chains.⁴² To our knowledge, there have been no reports for the polymer conformation in the ETFE amorphous

phase. Thus, it is difficult to determine if the relatively non-confined random coil-like structure originates from the amorphous lamellae in pristine ETFE or is induced by the preparation processes, graft-polymerization, *N*-alkylation, or swelling even though we ruled out the irradiation effects.

At $q < 0.09 \text{ nm}^{-1}$, $I(q)$ and q follow a power law function as $I(q) \sim q^{-2}$, seemingly indicating a lamellar structure, though no typical lamellar periodical peaks were observed at q_l in the profile. Note that the lamellar signature arising from the amorphous lamellar frame is always there, but apparently hidden by the tricky contrast matching technique.

IV-3 Morphology of crystalline ETFE domains. At m_2 ($f_{D2O} \sim 40\%$), the hydrated regions almost match the amorphous ETFE domains, thus the entire amorphous phase roughly has the same SLD, which makes the system automatically being simplified to a two-phase system: crystalline ETFE phase, and amorphous phase which includes all components such as graft chains, amorphous ETFE and water. The profile at m_2 , $I_{m2}(q)$, has been extracted and shown in Figure 7b. It reflects the morphology of crystalline ETFE domains. Since scattering patterns of hydrated regions in the amorphous lamellae has been hidden at this matching condition, a typical Porod law at high- q range is clearly observed, indicating the sharp interface between the crystalline ETFE domains and amorphous domains. The extracted profile for crystalline structures of ETFE at the matching condition is quite similar to the SAXS profiles of ETFE-PEMs with grafting degrees of 79-117%, in which amorphous hydrated and crystallite network domains appeared by graft- polymerization-induced phase transition of grafted ETFE.²² It should be noted that ETFE-PEM and AEM exhibit quite similar crystalline morphology although they are composed of different type of graft polymers (cation and anion conducting groups).

IV-4 Morphology of hydrated regions in the amorphous lamellae. Taking advantage of the contrast matching technique, we have successfully elucidated the morphologies of crystalline ETFE domains (phase 1) by the profile $I_{m2}(q)$ and hydrophobic amorphous ETFE domains

(phase 2) by the profile $I_{m1}(q)$. The only unclear domains left here are the hydrated regions (phase 3), which are found to be composed of entire graft chains and water, and have clear excess scattering at high- q range. In this section, we shall extract the excess scattering of these hydrated regions and elucidate their morphology in the amorphous phase.

For the current three-phase AEMs system, there is inhomogeneity within the individual phases, due to the atomic nature of the material and to the density fluctuations at all size scales arising from thermal motions of atoms. Thus, the total scattering intensity from such a system can be expressed by³⁹

$$I(q) = I_0(q) + I_1(q) + I_2(q) + I_3(q) + I_{12}(q) + I_{13}(q) + I_{23}(q) \quad (8)$$

where $I_0(q)$ is the background scattering, which has been corrected for each profile and can be neglected here. $I_1(q)$, $I_2(q)$ and $I_3(q)$ are the scattering due to the density fluctuations present independently in the three phases 1, 2 and 3, respectively. $I_{ij}(q)$ ($i, j = 1, 2, 3$) represents the effect associated with the interaction of the waves scattered in the different phases i and j . Since any correlation between the density fluctuations in the two phases across the phase boundaries is likely to be of short range, and consequently $I_{ij}(q)$ in this q -range is negligible. Thus eq. (8) is simplified to the eq. (9) below

$$I(q) = I_1(q) + I_2(q) + I_3(q) \quad (9)$$

It has been discussed above that the scattering profiles at matching points, m_1 and m_2 , *i.e.* $I_{m1}(q)$ and $I_{m2}(q)$ in Figures 7a and 7b represent the scattering from phase 2 and phase 1, respectively. In other words, $I_{m1}(q)$ and $I_{m2}(q)$ are $I_2(q)$ and $I_1(q)$ after contrast corrections at each f_{D2O} , respectively. Thus eq. (9) is converted to eq. (10) below

$$I(q) = (AI_{m2}(q) + BI_{m1}(q)) + I_3(q) \quad (10)$$

where A or B is the contrast factor, proportional to the square of the contrast between crystalline region and the entire amorphous region, or the one between amorphous ETFE and all the rest components in the sample, respectively. Thus all the profiles at $f_{D2O} > 55\%$ in Figure 3 can be fitted well by eq. (10). The best fitting curves are shown in the inset of Figure

7c, and the parameters A and B are listed in Table 2. The linear relationship between A or B and the related scattering contrast square has been verified and plotted in Figures S4 and S5 in the supporting information.

The excess scattering intensity of phase 3, $I_3(q)$, can be deduced from eq. (10) for each profile at $f_{D2O} > 55\%$. We plot $I_3(q)$ as a function of f_{D2O} in Figure 7c. Note that $I_3(q)$ for the profiles at $f_{D2O} \leq 20\%$ are too weak to be extracted accurately, and thus not shown in the figure.

A broad scattering maximum around $q_3 \sim 2.5 \text{ nm}^{-1}$ commonly shows up in $I_3(q)$ profiles in Figure 7c, indicating the density fluctuations of the graft chains present in the hydrated regions within the amorphous phase. According to the scattering theory, the scattering maximum at q_3 , $I(q_3)$, should be proportional to the square of the scattering contrast between graft chains (b_{graft}) and water, given by

$$I(q_3) \sim (b_{\text{graft}} - b_w)^2 \quad (11)$$

where $b_{\text{graft}} = \frac{\phi_{im}b_{im} + \phi_{st}b_{st}}{\phi_{im} + \phi_{st}} = 1.23 \times 10^{10} \text{ cm}^{-2}$, and b_w can be estimated by eq. (4). We plot $I(q_3)$ versus $(b_{\text{graft}} - b_w)^2$ for all $I_3(q)$ profiles at $f_{D2O} > 55\%$ in Figure 8, and a good linear relationship is clearly observed, evidencing that $I_3(q)$ profiles reflect the density fluctuations of the graft chains in the hydrated regions.

IV-5 GD dependence of the structure and property. In order to investigate the GD dependence of the structure and the property of the membranes, SANS measurements were also performed for grafted-ETFE membranes with GD of 30, 46 and 120% and the corresponding AEMs with $IECs$ of 0.95, 1.26 and 2.15 mmol/g, respectively (see SANS profiles in figure 6s in the supporting information). Though the shape of the scattering profiles are hardly changed in comparison with that of the membranes with a GD of 91%, the lamellar d -spacing varies significantly with the GD and water uptake in the membranes. In Figure 9a, the GD dependence of lamellar period, d_1 , for both grafted-ETFE membranes and AEMs

equilibrated in deuterated water at 25 °C are plotted. Additionally, the corresponding water uptake, U , for AEMs in the bicarbonate form is also plotted as a function of the GD in the inset of Figure 9a. A rapid increase in d_1 with the increase of GDs up to 46% is clearly observed for both membranes, and then d_1 changes steadily with the further increase in the GD. This is probably because at the early stage of graft polymerization, most graft chains were created within the lamellar stacks, while for higher GDs, graft chains were mainly generated outside of lamellar stacks due to the confined space. Thus, at the later stage of polymerization, d_1 of grafted-ETFE membranes does not change obviously though the GD continuously increases. This phenomenon was also observed in the ETFE and PTFE based PEMs prepared by the radiation grafting method, though the transition point of the GD, at which the lamellar d -spacing stopped increasing is variable, depending on the stiffness of the base film and the chemical structure of the grafts.²⁰⁻²² The increase in the GD definitely leads to the increase in U due to the more incorporation of hydrophilic imidazole groups. However, when the creation of the graft chains within lamellar stacks stopped, the water adsorption within the lamellar stacks would be restricted, too. Hence, the d_1 of AEMs also reaches a constant level, very similar to the case of grafted-ETFE membranes, though U gradually increases at higher GD levels (> 40%).

The hydroxide conductivity of these AEMs was measured in 1.0 M KOH solution at 60 °C, and plotted as a function of the GD in Figure 9b. High hydroxide conductivities over 100 mS/cm are observed for all of these AEMs. Generally, conductivities of ca. 100 mS/cm are the required level for high current density cell output.^{43,44} So far, the conductivity of the AEMs in the present study is the best in comparison with that of the recently reported AEMs formed by either poly(phenylene oxide) tethered with cationic alkyl side chains,⁴⁴ ionic liquid block copolymers,^{45,46} the block copolymer of polybutadiene-*b*-poly(4-methylstyrene)⁴⁷ or the polymer blends of the block copolymer of poly(vibylbenzyl chloride)-*b*-polystyrene and poly(2,6-dimethyl-1,4-phenylene oxide).⁴⁸ Figure 9b shows that the hydroxide conductivity

increases with increasing GDs. However, higher GDs over 100% usually result in too much higher water uptake, which causes poor stability and alkaline durability in a real fuel cell operation. The AEMs with GD = 120% were proved to be mechanically weak and own poor fuel cell performance, though their conductivity is higher than that of 2Me-AEM (GD = 91%, $IEC = 1.82$ mmol/g).

IV-6 Interplay between the morphology and property for AEMs. Let us next consider the interplay between the morphology and the property of the AEMs. According to the discussions above, the interconnected hydrated regions in the AEMs do exist, which are believed to play a key role to improve the ion conductivity of the membrane. 2Me-AEMs, which have the best well-balanced properties required for fuel cell applications exhibit a relatively high IEC value (1.82 mmol/g) in comparison with that of Nafion[®] membrane (0.91 mmol/g),⁴⁹ revealing a larger density of ionic groups in AEMs.^{50,51} This result is consistent with the SANS analysis in the sections above, which shows more pronounced hydrophilic/hydrophobic microphase separation than Nafion due to the incorporation of whole polymer grafts with the water composing the hydrated regions. On one hand, this leads to the high ion diffusion and water transport; on the other hand, the high ion exchange capacity leads to excessive swelling of polymer on hydration. However, the crystalline domains, consisting of crystalline and amorphous lamellae, originating from the substrate, can be conserved by preparation steps and water absorption; hence the concomitant loss of mechanical properties is restricted.

V. Conclusions.

In summary, for the first time, we employed contrast variation small angle neutron scattering technique to quantitatively investigate the morphology of the new graft-type AEMs: 2Me-PEM, composed of poly(dimethyl-vinylimidazole-co-styrene) copolymer chains grafted onto poly(ethylene-co-tetrafluoroethylene) films via radiation-induced grafting method. These AEMs were found to more or less conserve the crystalline lamellae and crystallites structures

from the pristine ETFE material, and hence possess the good mechanical properties and alkaline durability. After swelling in water, the interconnected hydrated conducting regions in the amorphous domains were formed, evidenced by the excess scattering at high- q range, and responsible for the high ion conductivity through the membranes. The contrast variation SANS studies on the AEMs, equilibrated in various water mixtures of water and deuterated water with different volume ratios, concluded that there exist three phases in these AEMs: phase 1) crystalline ETFE domains; phase 2) hydrophobic amorphous ETFE domains; and phase 3) interconnected hydrated domains, composed of the entire graft chains and water.

Acknowledgement.

This work was partially supported by the Advanced Low Carbon Technology Research and Development Program (ALCA) from the Japan Science and Technology Agency (JST).

References and Notes.

1. K. Yoshimura, H. Koshikawa, T. Yamaki, H. Shishitani, K. Yamamoto, S. Yamaguchi, H. Tanaka, Y. Maekawa, *J. Electrochem. Soc.*, 2014, **161**, F889.
2. W. Vielstich, A. Lamm, H. Gasteiger, *Handbook of Fuel Cells: Fundamentals, Technology, Applications*; John Wiley: 2004.
3. S.G. Chalk, J. F. Miller, F. W. Wagner, *J. Power Sources*, 2000, **86**, 40.
4. G. Cacciola, V. Antonucci, S. Freni, *J. Power Sources*, 2001, **100**, 67.
5. P. Costamagna, S. Srinivasan, *J. Power Sources*, 2001, **102**, 253.
6. A. F. Ghenciu, *Curr. Opin. Solid State Mater. Sci.*, 2002, **6**, 389.
7. S. Gamburgzev, A. J. Appleby, *J. Power Sources*, 2002, **107**, 5.
8. V. Mehta, J. S. Cooper, *J. Power Sources*, 2003, **114**, 32.
9. H. A. Gasteiger, J. E. Panels, *J. Power Sources*, 2004, **127**, 162.
10. M. Z. Jacobson, W. G. Colella, D. M. Golden, *Science*, 2005, **308**, 1901.
11. J. H. Wee, *Renewable & Sustainable Energy Reviews*, 2007, **11**, 1720.
12. Y. Wang, K. Chen, J. Mishler, S. C. Cho, X. C. Adroher, *Appl. Energy*, 2011, **88**, 981.
13. A. Serov, C. Kwak, *Appl. Catal. B: Environ.*, 2010, **98**, 1.
14. K. Asazawa, K. Yamada, H. Tanaka, A. Oka, M. Taniguchi, T. Kobayashi, *Angew. Chem., Int. Ed.*, 2007, **46**, 8024.
15. J. R. Varcoe, R. C. T. Slade, *Fuel Cells*, 2005, **5**, 187.
16. J. Pan, C. Chen, L. Zhuang, J. Liu, *Acc. Chem. Res.*, 2011, **45**, 473.
17. G. Couture, A. Alaaeddine, F. Boschet, B. Ameduri, *Prog. Polym. Sci.*, 2011, **36**, 1521.
18. G. Merle, M. Wessling, K. Nijmeijer, *J. Membr. Sci.*, 2011, **377**, 1.
19. H. Koshikawa, K. Yoshimura, W. Ainnananchi, T. Yamaki, M. Asano, K. Yamamoto, S. Yamaguchi, H. Tanaka, Y. Maekawa, *Macromol. Chem. Phys.*, 2013, **214**, 1756.
20. H. Iwase, S. Sawada, T. Yamaki, S. Koizumi, M. Ohnuma, Y. Maekawa, *Macromolecules*, 2012, **45**, 9121.

21. H. Iwase, S. Sawada, T. Yamaki, Y. Maekawa, S. Koizumi, *Inter. J. Polym. Sci.*, 2011, **1**.
22. T. D. Tap, S. Sawada, K. Hasegawa, Y. Yoshimura, M. Oba, M. Ohnuma, Y. Katsumura, Y. Maekawa, *Macromolecules*, 2012, **47**, 2373.
23. N. Li, T. Yan, Z. Li, T. T. Albrecht, W. H. Binder, *Energy Environ. Sci.*, 2012, **5**, 7888.
24. N. Li, Q. Zhang, C. Wang, Y.M. Lee, M. D. Guiver, *Macromolecules*, 2012, **45**, 2411.
25. F. Zhang, H. Zhang, C. Qu, *J. Mater. Chem.*, 2011, **21**, 12744.
26. H. Zhang, P. Shen, *Chem. Rev.*, 2012, **112**, 2780.
27. K. Mortensen, U. Gasser, S. A. Guersel, G. G. Scherer, *J. Polym Sci. Polym. Phys. Ed.*, 2008, **46**, 1660.
28. M. M. Nasef, E. A. Hegazy, *Prog. Polym. Sci.*, 2004, **29**, 499.
29. J. M. Song, B. S. Ko, J.Y. Sohn, Y. C. Nho, J. Shin, *Rad. Phys. Chem.*, 2014, **97**, 374.
30. A. Radulescu, V. Pipich, H. Frielinghaus, M. S. Appavou, *Journal of Physics: Conference Series*, 2012, **351**, 012026.
31. T. Ishigaki, A. Hoshikawa, M. Yonemura, T. Morishima, T. Kamiyama, R. Oishi, K. Aizawa, T. Sakuma, Y. Yomota, M. Arai, M. Hayashi, K. Ebata, Y. Takano, K. Komatsuzaki, H. Asano, Y. Takano, T. Kasao, *Nucl. Instr. Meth. Phys. Res. Sec. A*, 2009, **21**, 189.
32. K. Jokela, R. Serima, M. Torkkeli, F. Sundholm, T. Kallio, G. Sundholm, *J. Polym. Sci., Polym. Phys. Ed.*, 2002, **40**, 1539.
33. S. Balog, U. Gasser, K. Mortensen, L. Gubler, G. G. Scherer, H. B. Youcef, *Macromol. Chem. Phys.*, 2010, **211**, 635.
34. M. Reitman, D. Jaekel, R. Siskey, S. M. Kurtz, Chapter 4 –Morphology and Crystalline Architecture of Polyaryletherketones. in *PEEK Biomaterials Handbook*; ed. S. M. Kurtz, Elsevier Press, New York, 2012, pp 49.
35. T. W. Giants, *IEEE Trans. Dielectr. Insul.*, 1994, **1**, 991.
36. O. Dupont, A. M. Joneas, B. Nysten, R. Legras, P. Adriaensens, J. Gelan, *Macromolecules*,

- 2000, **33**, 562.
37. G. Gebel, *Macromolecules*, 2013, **46**, 6057.
 38. V. Di Noto, M. Piga, G. A. Giffin, G. Pace, *J. Membr. Sci.*, 2012, **390-391**, 58.
 39. See for example, R. J. Roe, *Methods of X-ray and neutron scattering in polymer science*, Oxford Uni. Press, New York, 2000.
 40. Since the ratio of ET to FE in the commercial ETFE membranes is 1:1, the SLD of the amorphous ETFE ($b_{\text{amo_ETFE}}$) can be calculated by the volume averaged SLD of amorphous ET ($b_{\text{amo_ET}}$) and amorphous FE ($b_{\text{amo_FE}}$) as follows: $b_{\text{amo_ETFE}} = \frac{1}{2}(b_{\text{amo_ET}} + b_{\text{amo_FE}})$. The mass density of amorphous ET ($d_{\text{amo_ET}}$) and FE ($d_{\text{amo_FE}}$) are generally assumed to be 0.86 and 2.0 g/cm³, respectively. Thus $b_{\text{amo_ET}}$ and $b_{\text{amo_FE}}$ are theoretically calculated to be -0.306 and 4.33 ($\times 10^{10} \text{ cm}^{-2}$), respectively. Hence $b_{\text{amo_ETFE}}$ is estimated to be $2.0 \times 10^{10} \text{ cm}^{-2}$. Similarly, SLD of D₂O and H₂O are theoretically calculated to be 6.34 and -0.56 ($\times 10^{10} \text{ cm}^{-2}$), respectively, the values of which will be used in the following sections to discuss the matching point.
 41. G. Porod, *Kolloid Zeit*, 1951, **124**, 83.
 42. A. Oshima, S. Ikeda, T. Seguchi, Y. Tabata, *Radia. Phys. Chem.*, 1997, **50**, 519.
 43. J. R. Varcoe, P. Atanassov, D. R. Dekel, A. M. Herring, M. A. Hickner, P. A. Kucernak, W. E. Mustain, K. Nijmeijer, K. Scott, T. W. Xu, L. Zhuang, *Energy Environ. Sci.*, 2014, **7**, 3135.
 44. H. S. Dang, P. Jannasch, *Macromolecules*, 2015, **48**, 5741.
 45. Y. Ye, S. Sharick, E. M. Davis, K. I. Winey, Y. A. Elabd, *ACS Macro Lett.*, 2013, **2**, 575.
 46. K. M. Meek, S. Sharick, Y.S. Ye, K. I. Winey, Y. A. Elabd, *Macromolecules*, 2015, **48**, 4850.
 47. Y.F. Li, Y. Liu, A. C. Jackson, F. L. Beyer, S. Seifert, A. M. Herring, D. M. Knauss, *Macromolecules*, 2015, **48**, 6523.

- 48. Y.F. Li, A. C. Jackson, F. L. Beyer, D. M. Knauss, *Macromolecules*, 2014, **47**, 6757.
- 49. K. A. Mauritz, R. B. Moore, *Chemical Reviews*, 2004, **104**, 4535.
- 50. O. Diat, G. Gebel, *Nature Materials*, 2008, **7**, 13.
- 51. G. Gebel, J. Lambard, *Macromolecules*, 1997, **30**, 7914.

Figure caption

Scheme 1 Molecular structure of the 2Me-AEMs used in this study.

Figure 1 SANS profiles measured for pristine ETFE membranes (open squares), grafted-ETFE (open circles), dry 2Me-AEMs (open down-triangles) and fully D₂O swollen 2Me-AEMs (open up-triangles) at room temperature.

Figure 2 Schematic illustrations of the morphology of (a) dry pristine ETFE membranes; (b) dry grafted ETFE membranes or AEMs; (c) AEMs equilibrated in water.

Figure 3 SANS profiles (symbols) obtained from 2Me-AEMs equilibrated in water mixture with different representative f_{D2O} .

Figure 4 f_{D2O} dependence of Part (a): the scattering maximum at q_I ($= 0.185 \text{ nm}^{-1}$), $I(q_I)$; Part (b): the scattering intensity at q_{II} ($= 2.0 \text{ nm}^{-1}$), $I(q_{II})$, observed for AEMs swollen in water mixtures shown in Figure 3. Inset of Part (a): Schematic illustration for phase matching at m_1 . Inset of Part (b): Schematic illustration for phase matching at m_2 .

Figure 5 Normalized SANS profiles by the typical crystalline peak at q_I ($= 0.185 \text{ nm}^{-1}$).

Figure 6 Plot of $I(q_I)$ versus $(b_{cry_ETFE} - b_{amo})^2$ for profiles of AEMs equilibrated in water mixtures where the components of hydrated regions are made of entire graft chains and water, and b_{cry_ETFE} is $2.23 \times 10^{10} \text{ cm}^{-2}$. The inset: Schematic illustrations of the components of hydrated regions (regions with painting), which are composed of the entire graft chains (both imidazole and styrene segments are included) and water;

Figure 7 Part (a): SANS profile of amorphous ETFE domains (profile at the matching point of m_1). The best-fitted curve based on eq. (7) at high- q range ($q > 0.09 \text{ nm}^{-1}$) is shown in the figure by solid line, and the straight line at low- q range ($q < 0.09 \text{ nm}^{-1}$) is also drawn to guide the readers' eyes; Part (b): SANS profile of crystalline ETFE domains (profile at the matching point of m_2); Part (c): SANS

profiles of the hydrated domains, $I_3(q)$, at $f_{D2O} > 55\%$. Inset of Part (c): The comparison between the profiles at $f_{D2O} > 55\%$ (symbols) and the theoretical curves (solid lines) based on eq. (9) through all q -range.

Figure 8 Plot of $I(q_3)$ versus $(b_{graft} - b_w)^2$ for profiles of hydrated regions shown in Figure 8c according to eq. (11).

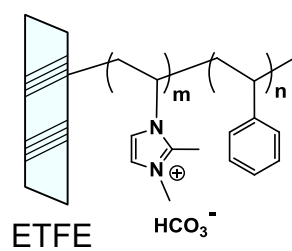
Figure 9 GD dependence of part (a) lamellar period (d_l), the inset of part (a) water uptake (U); Part (b) ion conductivity in 1.0 M KOH at 60 °C.

Table 1 Scattering length density (b) and the volume fraction (ϕ) of each component in the AEMs equilibrated in water.

	cry_ETFE	amo_ETFE	St	im	water
$b (\times 10^{-10} \text{ cm}^{-2})$	2.23	2.0	1.415	1.123	variable
$\phi (\%)$	7.55	16.05	13.82	24.58	38

Table 2 Contrast factors used in eq. (10) for all profiles at $f_{\text{D2O}} > 55\%$.

f_{D2O}	70%	80%	90%	100%
A	0.7	2.1	4.2	7
B	2.0	3.5	5.6	8.2



Scheme 1

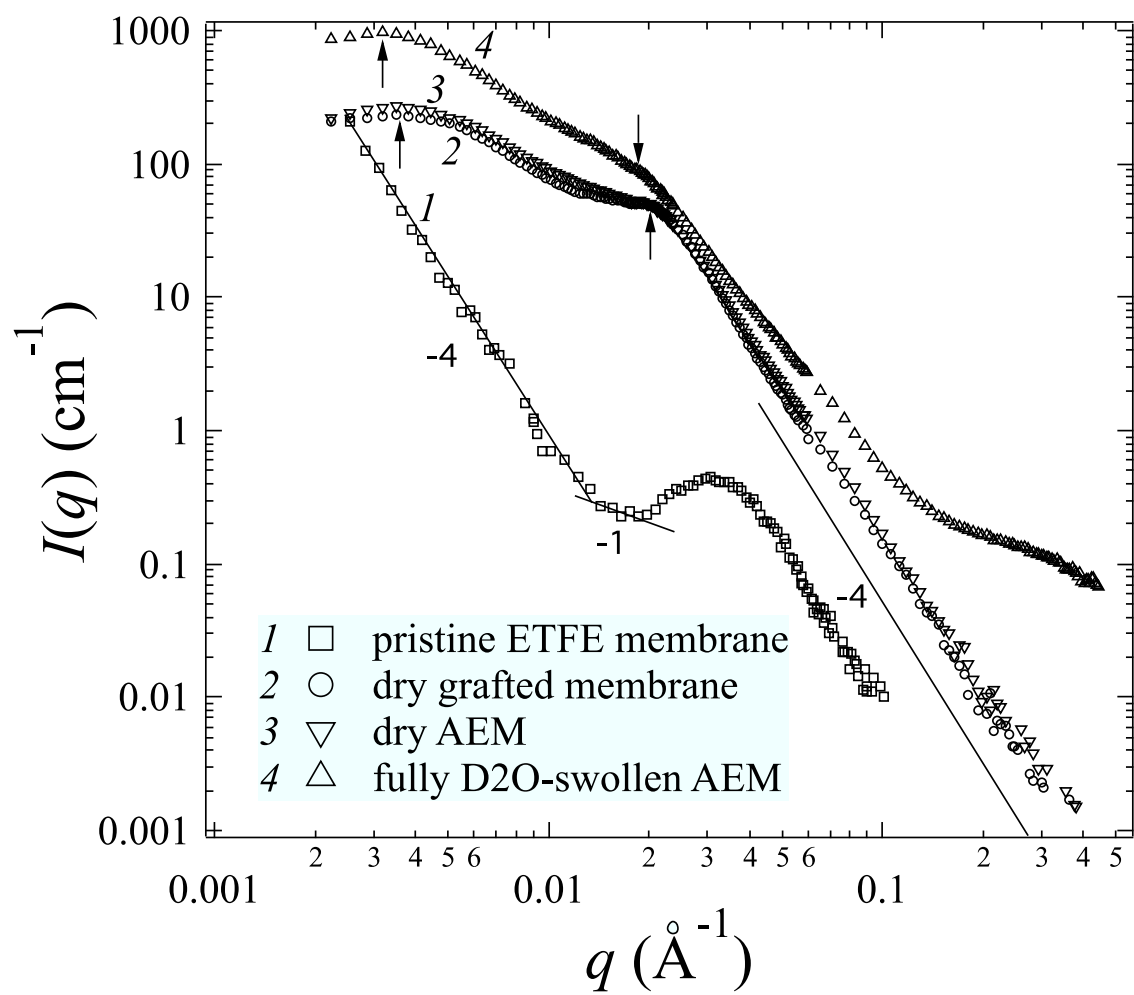


Figure 1

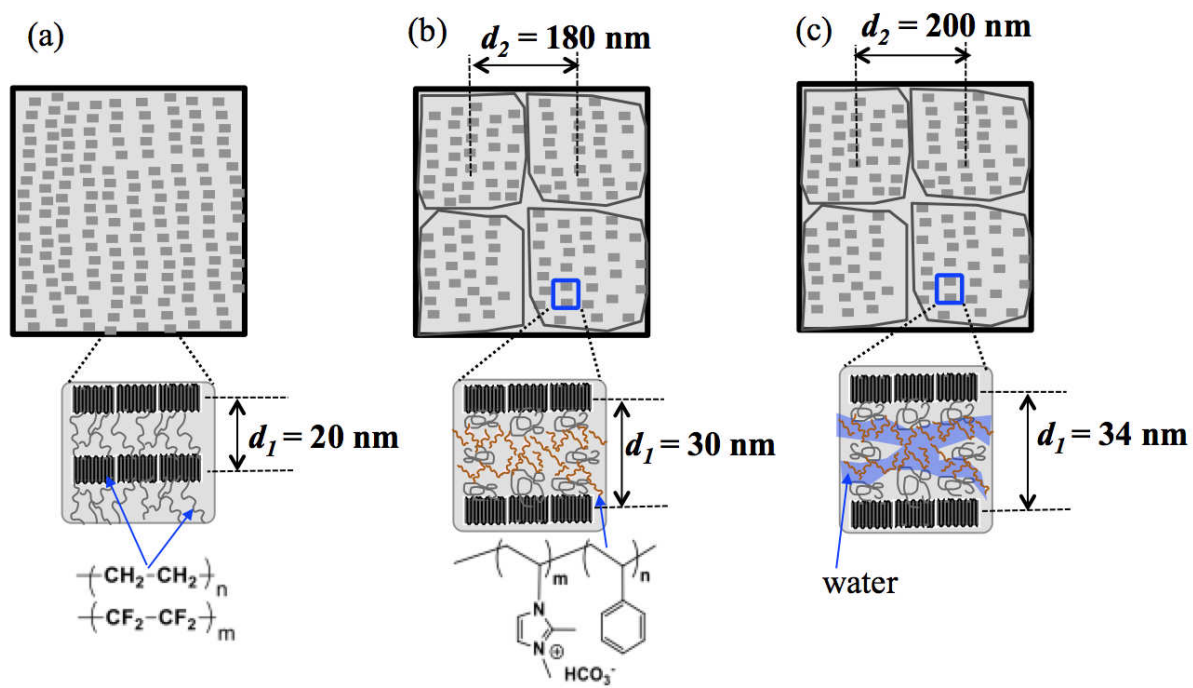


Figure 2

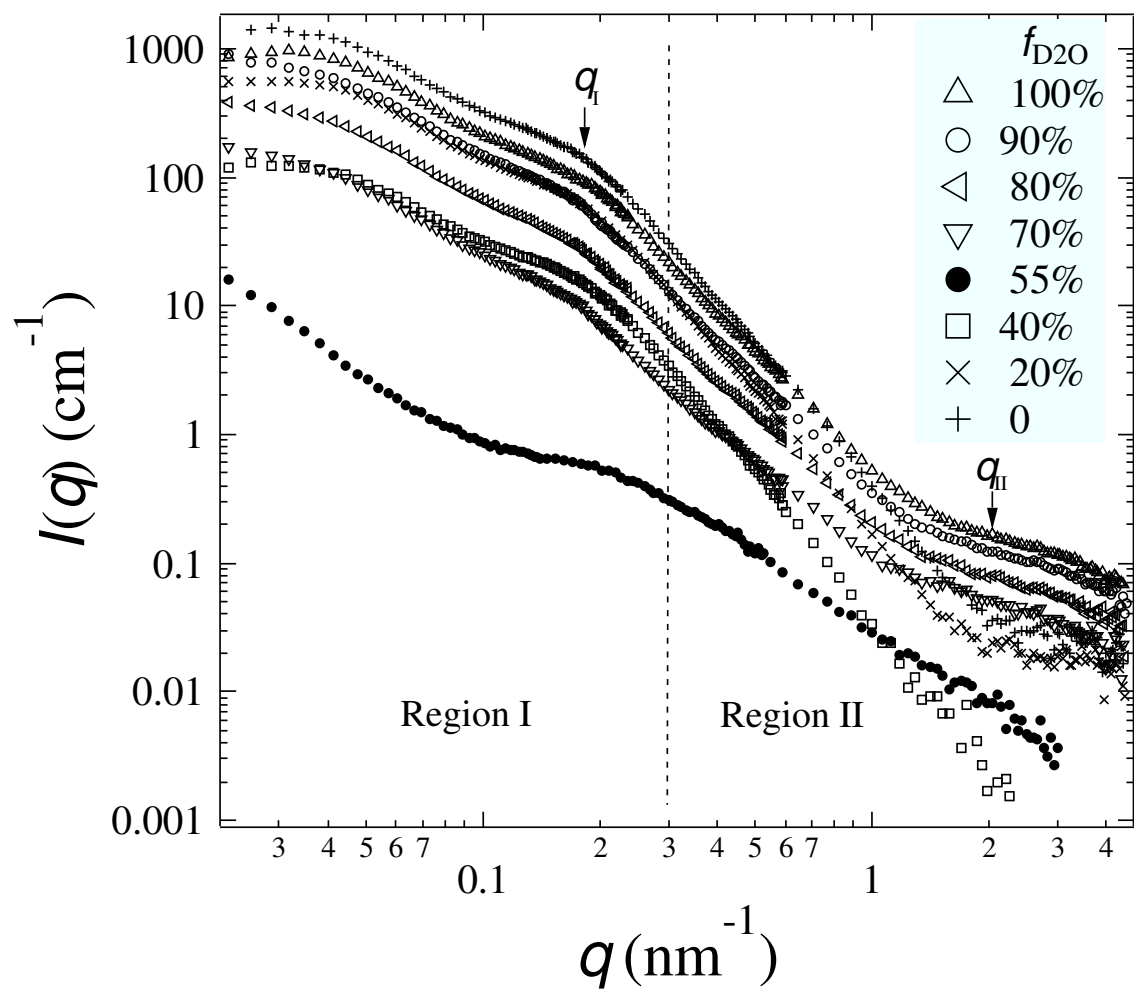


Figure 3

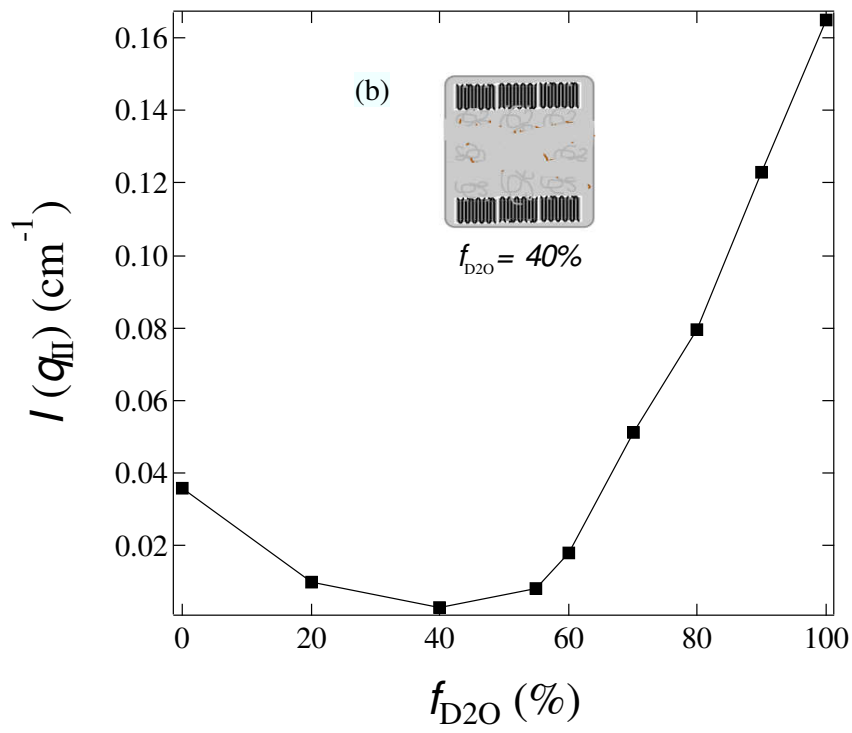
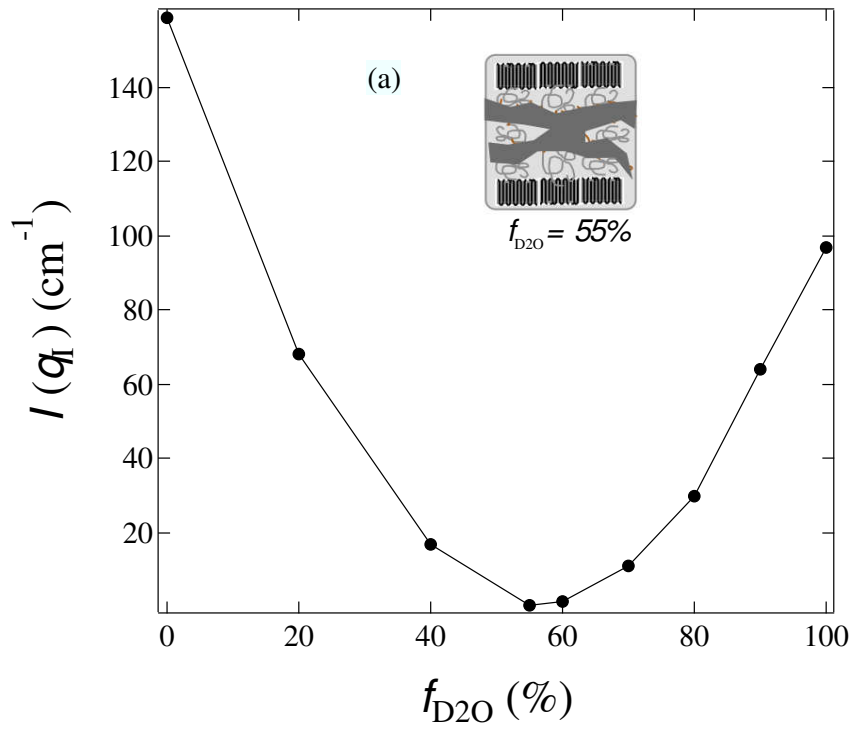


Figure 4

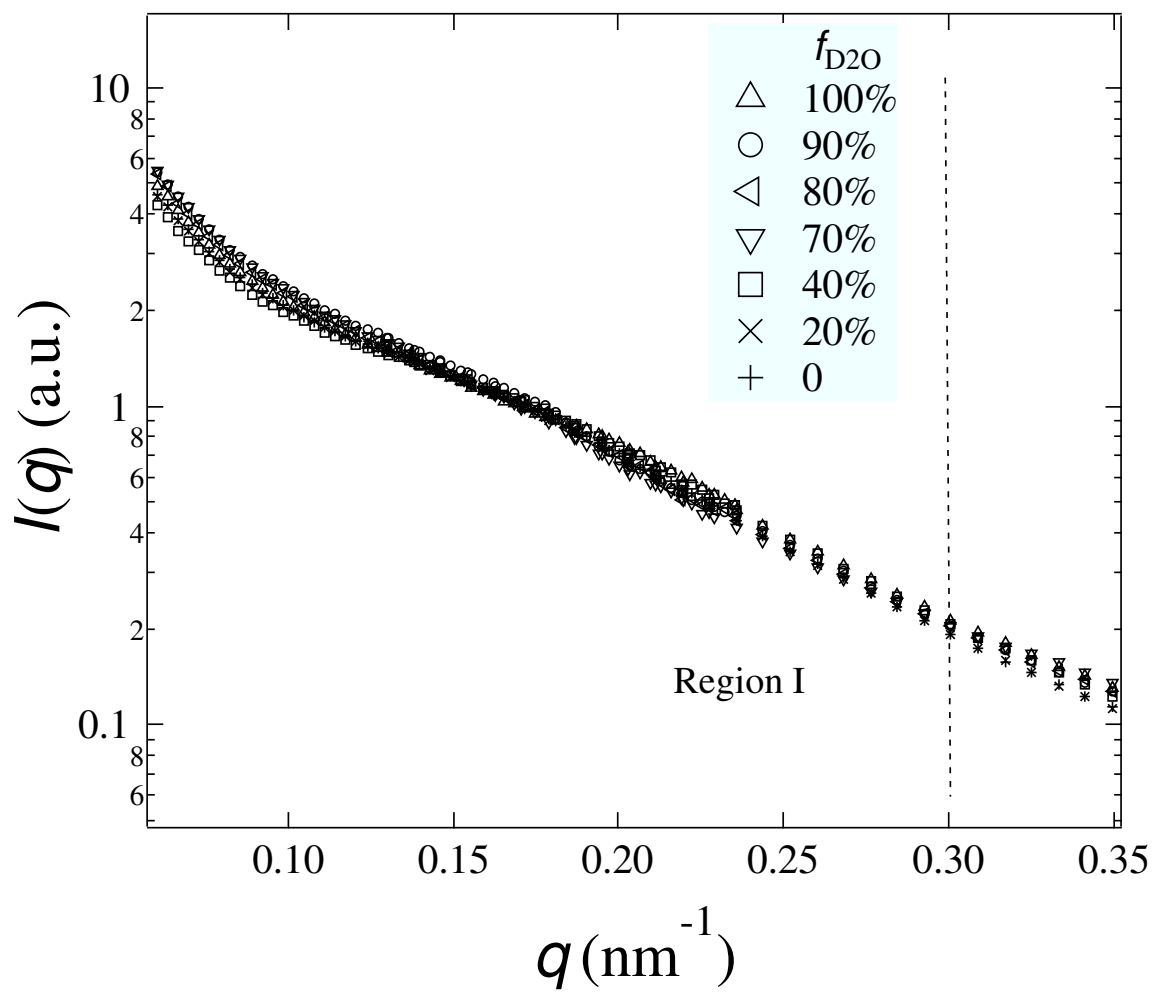


Figure 5

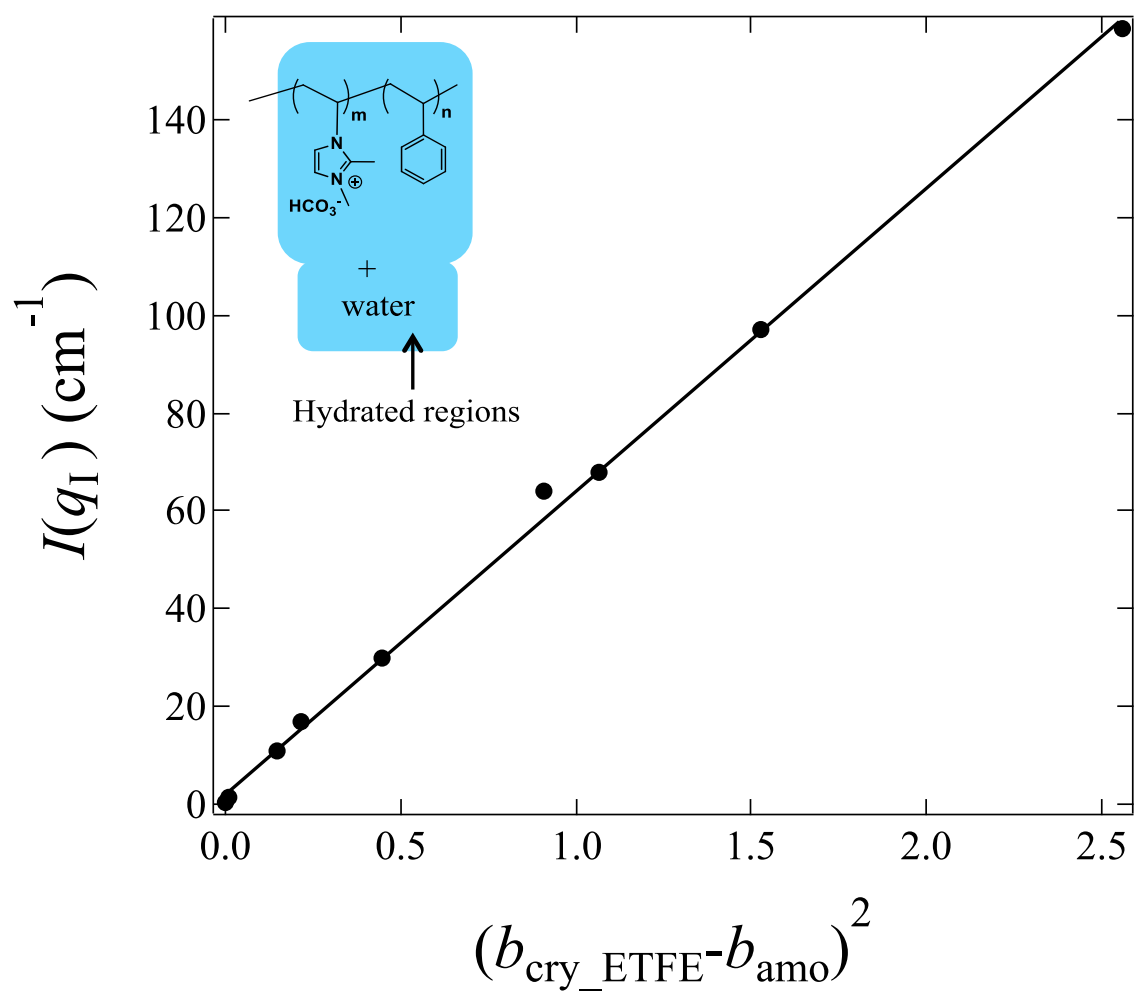


Figure 6

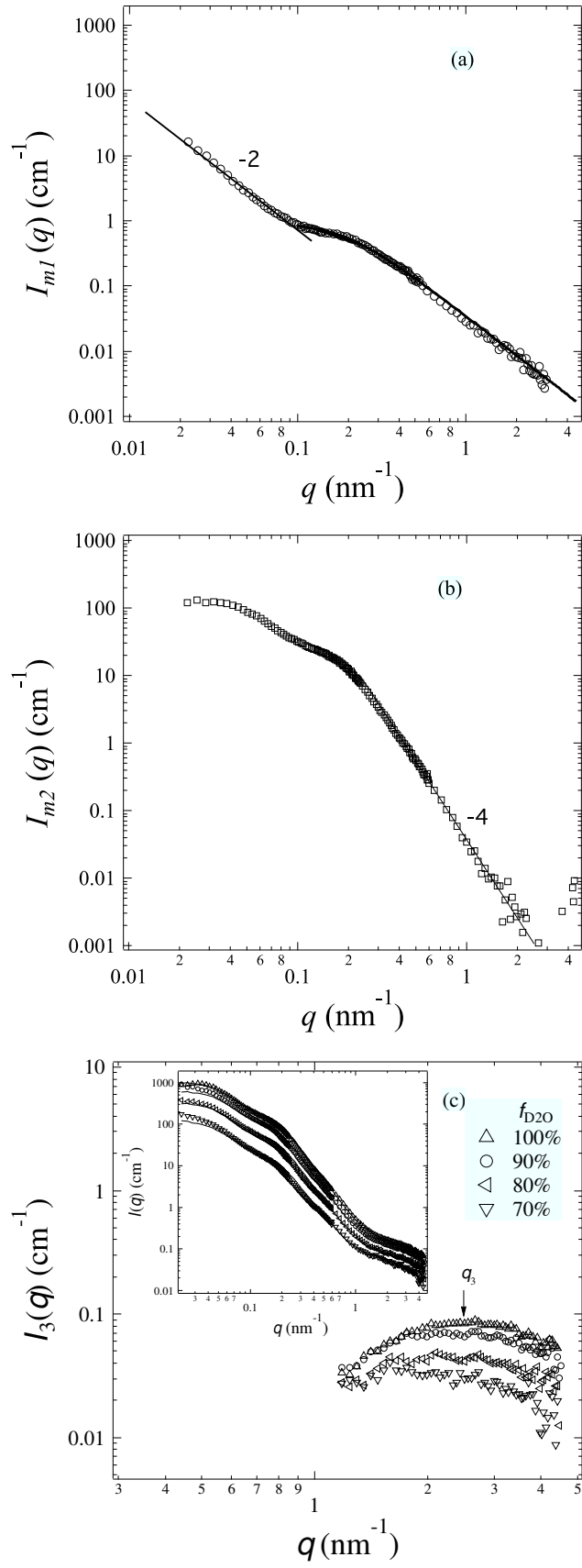


Figure 7

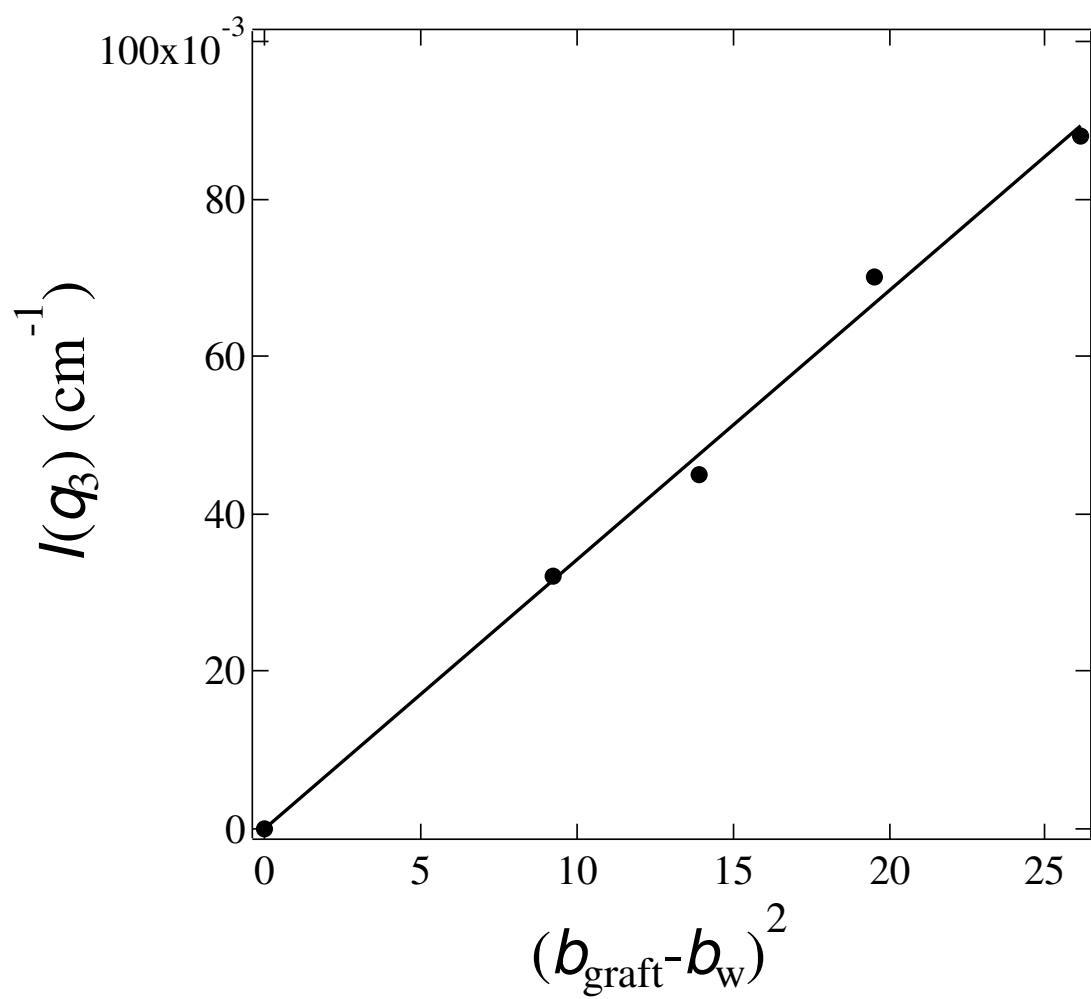


Figure 8

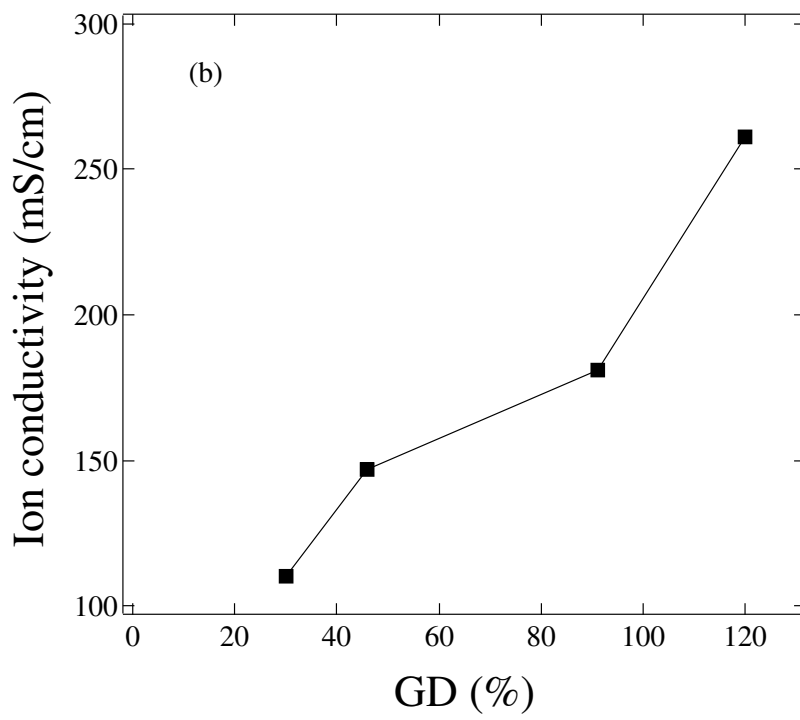
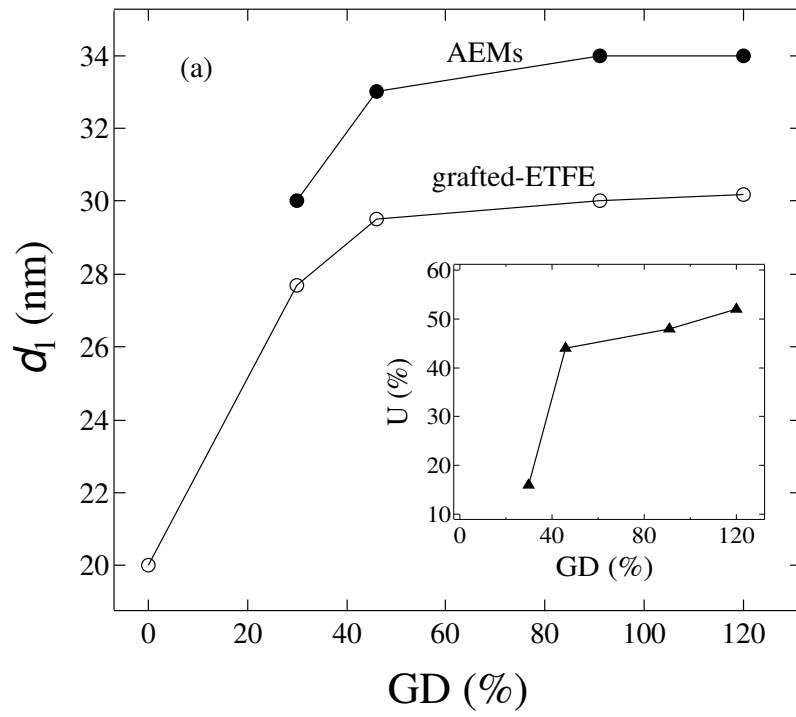


Figure 9

Imidazolium-Based Anion Exchange Membranes For Alkaline Anion Fuel Cells: Elucidation of the Morphology and the Interplay Between Morphology and Properties

Yue Zhao,^{1,*} Kimio Yoshimura,¹ Hideyuki Shishitani,² Susumu Yamaguchi,² Hirohisa Tanaka,² Satoshi Koizumi,^{3,*} Noemi Szekely,⁴ Aurel Radulescu,⁴ Dieter Richter,⁵ Yasunari Maekawa^{1,*}

¹*Quantum Beam Science Center (QuBS), Japan Atomic Energy Agency (JAEA), Tokai-mura, Ibaraki, 319-1195, and Takasaki 1233, Gunma, 370-1292, Japan*

²*Daihatsu Motor Co., Ltd., Ryuo Gamo, Shiga 520-2593, Japan*

³*Department of Engineering, Ibaraki University, Hitachi 316-8511, Japan*

⁴*Forschungszentrum Jülich GmbH, Jülich Centre for Neutron Science @ MLZ, Lichtenbergstraße 1, D-85747 Garching, Germany*

⁵*Jülich Centre for Neutron Science & Institute for Complex Systems, Forschungszentrum Jülich GmbH, D-52425 Jülich, Germany*

Table of Contents Graphic

